Science Bulletin 64 (2019) 1409–1417

Contents lists available at ScienceDirect

Science Bulletin

journal homepage: www.elsevier.com/locate/scib

Science Bulletin
www.scibull.com

Article

A water-evaporation-induced self-charging hybrid power unit for application in the Internet of Things

Haoxuan He [a,b], Tianming Zhao [a,b], Hongye Guan [a,b], Tianyan Zhong [a,b], Hui Zeng [b], Lili Xing [a,b,*], Yan Zhang [a], Xinyu Xue [a,b,*]

[a] School of Physics, University of Electronic Science and Technology of China, Chengdu 610054, China
[b] College of Sciences, Northeastern University, Shenyang 110819, China

ARTICLE INFO

Article history:
Received 19 April 2019
Received in revised form 3 June 2019
Accepted 17 June 2019
Available online 22 June 2019

Keywords:
Self-charging
Hybrid power unit
Water evaporation
Nanogenerator
Supercapacitor
Internet of Things

ABSTRACT

A self-charging hybrid power unit has been developed by integrating a water-evaporation-induced nanogenerator with a flexible nano-patterned supercapacitor. The nanogenerator can harvest environmental thermal energy and mechanical energy through the water evaporation process, and the supercapacitor can be charged simultaneously. The former offers stable electrical power as output, whereas the Ppy-based supercapacitor shows a capacitance of 12.497 mF/cm^2 with 96.42% retention after 4,000 cycles. After filling the power unit with water as the fuel, it can be fully charged in about 20 min. The power unit can be flexibly integrated with electronic devices such as sensor nodes and wireless transmitters employing the Internet of Things. This new approach can offer new possibilities in continuous future operation of randomly distributed electronic devices incorporated in the Internet of Things.

© 2019 Science China Press. Published by Elsevier B.V. and Science China Press. All rights reserved.

1. Introduction

The Internet of Things (IoT) refers to the concept of extending internet connectivity beyond conventional computing platforms to a variety of traditionally physical devices and everyday objects [1–4]. The extensive range of applications offered by the IoT can significantly improve our lives, including the consumer, commercial, industrial, and infrastructure aspects. Incorporating electronics, internet connectivity, and various sensor nodes, these devices can communicate and interact with other such connected devices on the internet. In terms of collecting and transmitting data whenever and wherever, attempts have been made to ensure that electronic devices applicable in the IoT are smaller, lighter, thinner, more flexible, and even capable of rolling up [5–9]. The traditional cumbersome power unit embedded in the system raises the maintenance costs and complexity of the system and impedes the widespread application of the IoT (the sensing nodes and other electronic devices are usually distributed randomly) [10–14]. Commercial batteries/capacitors suffer from the drawbacks of limited lifetime and the need for frequent replacement [15–19]. A self-sustainable battery-free data collection/transmission system driven by the energy available from the surroundings could promote further development of the IoT [20–24].

Over the past decades, many researchers have explored highly efficient energy conversion devices for constructing battery-free self-powered systems such as piezoelectric or triboelectric nanogenerators [25–31]. Most recently, a new water-evaporation-induced nanogenerator has been reported [32,33]. Through the coupling effect between streaming potential and a natural water evaporation process on the surface of nano-carbon films, the nanogenerator can efficiently harvest environmental thermal and mechanical energy [34–36]. Considering the abundance of water on the earth, the water-evaporation-induced nanogenerator is an ideal power source for integrating with electronic devices in the IoT. For long-term operation of the system and flexible use of energy, energy storage is also necessary. Supercapacitors, an important class of energy storage devices, offer high power density and long cycling life [37–42]. Such energy harvesting and storage technologies have developed independently [43]. Recently, many groups have reported a series of self-charging hybrid power units with novel fundamental mechanisms that directly hybridize the energy conversion and storage processes into one [44–51].

In this work, a new self-charging hybrid power unit has been developed by integrating a water-evaporation-induced nanogenerator with a flexible nano-patterned supercapacitor. The power unit can directly convert and store environmental thermal energy and

* Corresponding authors.
E-mail addresses: xinglili@mail.neu.edu.cn (L. Xing), xuexinyu@mail.neu.edu.cn (X. Xue).

https://doi.org/10.1016/j.scib.2019.06.020
2095-9273/© 2019 Science China Press. Published by Elsevier B.V. and Science China Press. All rights reserved.

mechanical energy. The electricity generated by water evaporation can simultaneously charge the supercapacitor. The water can be treated as the fuel of the power unit, which can be flexibly integrated with sensor nodes and wireless transmitters to establish a self-powered sensing system in the IoT. This new approach provides an innovative route toward further development of the IoT.

2. Experimental

2.1. Preparation of water-evaporation-induced nanogenerator

The first step was to prepare porous carbon slurry. Toluene soot was obtained using a flame synthesis experiment carried out using a common alcohol burner filled with toluene. A quartz substrate was used for collection of the soot and no catalyst was used. During the synthesis, the quartz substrate was maintained in the toluene vertical flame zone (5.5 cm above the center cone). The synthesis time was about 5 min. Then, the quartz substrate was removed from the flame, and the toluene soot was collected. The toluene soot, ethyl cellulose, and terpineol were mixed in a mass ratio of 1:2:6 and 1 g of the mixture was added to 100 mL of ethanol under magnetic stirring for 4 h in an oil bath at 60 °C to form uniform carbon slurry.

The Kapton film is used as a flexible substrate for coating photoresists and electron beam deposition extensively because of its excellent thermostability, inherent strength, and insulation properties [52,53]. Kapton boards were ultrasonically cleaned in acetone, ethanol, and deionized water for several times and then dried at 60 °C. Then, the commercial carbon nanotube (CNT) ink was printed on the Kapton board as an electrode (width of 4 mm). Two electrodes were printed on the edge of the Kapton board. The porous carbon slurry was printed on the Kapton board crossing the two electrodes, and the printing process was repeated three times to ensure a certain thickness. The as-printed Kapton board was then dried at 60 °C for 0.5 h, annealed at 375 °C for 2.5 h in ambient atmosphere, and allowed to cool to room temperature, which occurred spontaneously. Finally, the bare electrode area of the nanogenerator was wired and carefully covered by epoxy and dried at 60 °C for 3 h.

2.2. Preparation of flexible Ppy-based nano-patterned supercapacitor

The flexible nano-patterned supercapacitor was prepared by photolithography, electron beam evaporation, and electrochemical polymerization. First, the Kapton board was cleaned with deionized water, ethanol, and acetone several times to remove surface impurities. Then, the Kapton board was heated for 150 s at 80 °C. 5 mL of a positive photoresist (RZJ-304, 25 mPa s, Suzhou Ruihong Co., Ltd.) was spin-coated on the Kapton board at 200 r/min for 40 s and at 1,500 r/min for 90 s and then dried at 100 °C for 150 s. Next, the Kapton board was exposed to UV light (365 nm) for 2.4 s to cure the positive photoresist in the photolithography machine (H94-17G, Sichuan Nanguang Co., Ltd.). The thickness of cured positive photoresist was 0.8 μm. A pre-designed interdigital electrode pattern was obtained on the Kapton board. The Kapton film with the cured positive photoresist was then immersed into a developer in a petri dish, which was shaken for 60 s, following which the Kapton board was washed with deionized water and dried under N_2 flow. The prepared Kapton film was hardened at 120 °C for 150 s. All of steps in the photolithographic process were conducted in the darkroom. A Ni film with a thickness of 200 nm was then coated on the Kapton board by electron beam evaporation. Finally, the Kapton board was immersed in acetone to remove the cured positive photoresist and redundant Ni film and washed with deionized water and dried at 60 °C. Thus, a Ni interdigital electrode on the Kapton board was obtained.

Ppy was grown on the Ni interdigital electrode through electrochemical polymerization using an electrochemical workstation (CHI627D, CH Instruments, Inc.). The Kapton board with the Ni interdigital electrode was immersed in a 50 mL solution containing 0.1 mol/L pyrrole monomer and 0.2 mol/L oxalate acid as the dopant. Electrochemical polymerization was carried out under a constant voltage of 0.8 V in a three-electrode system for 200 s, wherein the Ag/AgCl electrode and a Pt sheet were used as the reference electrode and counter electrode, respectively. After polymerization, the Kapton board with the as-fabricated Ppy on the Ni interdigital electrode was taken out and washed with deionized water.

The Ppy-based supercapacitor was fabricated by casting the polyvinyl alcohol (PVA)/H_3PO_4 gel electrolyte. The gel electrolyte was prepared by adding 1 g of PVA and 1 g of H_3PO_4 into 10 mL of deionized water. The solution was stirred for 4 h at 80 °C. The solution was slowly cooled to room temperature to form the gel electrolyte, which was subjected to vacuum treatment thrice to eliminate the bubbles in the gel.

2.3. Fabrication of self-charging hybrid power unit

The flexible nano-patterned supercapacitor and water-evaporation-induced nanogenerator were integrated on a Kapton board, forming a self-charging hybrid power unit and were connected by a printed CNT electrode. The power unit was placed on a polydimethylsiloxane (PDMS) layer in a pre-cleaned PMMA box. The PDMS mixture was prepared by mixing the elastomer and crosslinker in a mass ratio of 10:1 and ultrasonically treating it for 20 min and then vacuum treating it for 20 min to eliminate the bubbles in the PDMS mixture. Then, this PDMS mixture was slowly dropped in the PMMA mold box. Another layer of liquid PDMS mixture was poured onto the supercapacitor and the connected electrodes to cover and protect the power unit. After heating in vacuum at 90 °C for 1.5 h, the entire power unit was lifted off the PMMA mold box.

2.4. Characterization and measurements

The morphology and structure of the power unit were investigated by scanning electron microscopy (SEM, Hitachi S4800). Electrochemical tests were carried out on an electrochemical workstation (CHI627D, CH Instruments, Inc.). The charging/discharging performance of the supercapacitor was monitored by a battery measurement system (BST-TC53, MTI Company). The output current and voltage of the nanogenerator under different conditions was studied by a low-noise current preamplifier (Model SR570, Stanford Research Systems) and a Keithley 2002 multimeter, respectively. The wireless transmitter used was a XKFST. The working voltage and frequency were about 3–12 V and 315 Hz, respectively. The transmission speed was 4 kb/s. The working temperature range was about −10 to +70 °C. The length of the outside antenna and transmitting distance were about 25 cm and 50–200 m, respectively. All the experimental measurements were conducted under a pressure of 1.01×10^5 Pa at room temperature (25 °C).

3. Results and discussion

Fig. 1a shows potential application of the self-charging hybrid power unit as part of the IoT. Different electronic devices and sensor nodes in the IoT can communicate and interact with others over the internet. For collecting and transmitting data, a large

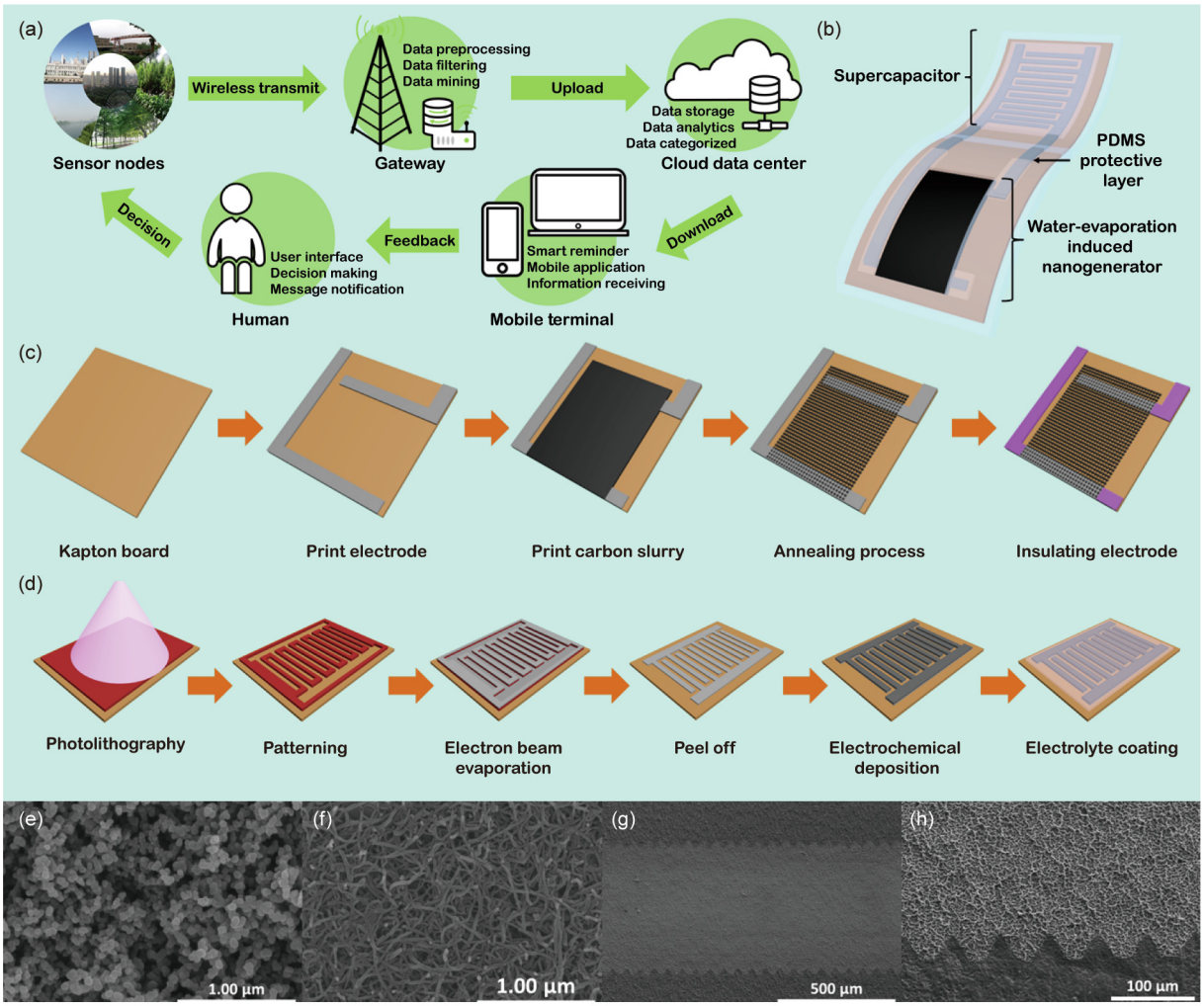

Fig. 1. (Color online) Experimental design of self-powered hybrid power unit. (a) Application of self-charging hybrid power unit in the IoT. (b) Design of the power unit. (c) Fabrication of water-evaporation-induced nanogenerator. (d) Fabrication of flexible nano-patterned supercapacitor. (e) SEM image of the porous carbon film. (f) SEM image of the CNTs. (g, h) Morphology of Ppy.

number of sensor nodes and wireless transmitters are usually integrated in one system. The data are wirelessly transmitted to the gateway for preprocessing and then uploaded to the cloud. After analyzing and computing in the cloud, people can download useful data from the internet. In terms of collecting and transmitting data whenever and wherever, the water-evaporation-induced self-charging hybrid power unit can be integrated in the system to form a self-powered sensing/transmitting system in the IoT. The power unit is filled with water as the fuel, and the water evaporation process can harvest environmental thermal energy and mechanical energy and store it for powering the system. This self-sustainable battery-free data collection/transmission system can facilitate popularization of the IoT.

Fig. 1b represents a schematic illustration of the structure of the self-charging hybrid power unit, which composed of a water-evaporation-induced nanogenerator, a flexible nano-patterned supercapacitor, and a protective PDMS layer. Fig. S1 (online) shows a digital photograph of the nanogenerator, supercapacitor, and entire power unit. The nanogenerator and supercapacitor are connected with the printed CNT electrode, and the CNT electrodes and supercapacitor are sealed with the PDMS layer, which can protect the entire power unit. Leakage of the electrolyte in the supercapacitor is prevented by sealing with the PDMS layer, which shows excellent flexibility that enables the entire power unit to be easily bent. The flexible power unit can be placed everywhere and even be attached to the human body.

The fabrication process of the self-charging hybrid power unit is schematically shown in Fig. 1c and d. Fig. 1c illustrates the synthesis of the water-evaporation-induced nanogenerator. The commercial CNT ink was first printed as electrodes on a pre-cleaned Kapton board. Then, the porous carbon slurry—prepared by mixing toluene soot, ethyl cellulose, and terpineol—was painted across the two CNT electrodes. The bare electrodes were covered by epoxy to avoid exposure of the electrodes to water, and the water-evaporation-induced nanogenerator was prepared. Fig. S1a (online) shows the digital photograph of a typical nanogenerator with a size of (5×5) cm^2. Fig. 1d schematically shows the fabrication of the flexible nano-patterned supercapacitor. Pre-designed interdigital Ni electrodes were obtained on the Kapton board by photolithography and electron beam evaporation. The cured photoresist and redundant Ni film were peeled off by immersing the Kapton board in acetone. Ppy was coated on the Ni electrodes by electrochemical polymerization. The supercapacitor was filled with a gel electrolyte (PVA/H_3PO_4) and sealed compactly with PDMS. Fig. S1b (online) shows a digital photograph of the nano-patterned supercapacitor.

SEM images of the porous carbon film after annealing were obtained at different magnifications (Figs. 1e and S2 (online)),

indicating that the porous carbon film was composed of interconnected carbon nanoparticles of uniform size. The average diameter of the carbon nanoparticles was about 80 nm. Figs. 1f and S3 (online) show the SEM images of the CNT electrode under different magnifications. Figs. S4 and S5 (online) show the side-view SEM images of the porous carbon film and CNT electrode after annealing. The thicknesses of the porous carbon film and CNT electrode were 15 and 5 μm, respectively. Digital photographs of the nanogenerator under applied deformation and SEM images of the nanogenerator after bending for 500 times are shown in Fig. S6 (online). No sharp creases could be seen on the porous carbon film even after repeated bending, which demonstrated the excellent flexibility of the nanogenerator. Figs. 1g, h, S7 and S8 (online) show that Ppy was deposited on the Ni electrodes and microstructural investigation of the Ppy film confirmed that there were no pores or fractures on its surface. The width of the Ppy electrode was about 500 μm.

The energy conversion performance of the water-evaporation-induced nanogenerator was investigated, as shown in Fig. 2. Fig. S9 (online) shows the working process of the water-evaporation-induced nanogenerator. The nanogenerator was first fully infiltrated with water. It was placed in a 100 mL beaker with water (the water level was higher than the level of the bottom electrode). The bottom CNT electrode acted as the negative electrode during the test, and the top one acted as the positive electrode. The working principle of the water-evaporation-induced nanogenerator is shown in Fig. 2a. The porous carbon film was composed of interconnected carbon nanoparticles with nanometer-sized pores. When water contacted the porous carbon film, an overlapped electric double layer was formed spontaneously at the carbon-water interface. The capillary force and evaporation drove the water flow uphill through the porous carbon film [54–57]. The zeta potential of the porous carbon film was about −27.21 mV (Fig. S10 online). Thus, the hydroxide ions in the water flow were repelled, resulting in excess hydronium ions carried by the water flow uphill [32–35]. This process resulted in a streaming current and created a higher potential at the top electrode. The zeta potential reached a constant value and the water level was stable. The hydronium ions carried uphill cannot accumulate infinitely. When the charge transfer in carbon materials reached a state of dynamic equilibrium, hydronium ions reached a certain concentration and the output voltage reached a stable value. An open-circuit voltage (V_{oc}) was generated between the two CNT electrodes and gradually increased in value to about 1.2 V in a short period (upper curve in Fig. 2b). The output voltage was maintained steadily during the test at room temperature (25 °C) and 30% relative humidity (RH). When the nanogenerator was turned over (the other end was dipped into the water without changing any of the electric connections), the voltage reversed its sign but reached the same amplitude (lower curve in Fig. 2b). A short-circuit current (I_{sc}) of 0.5 μA was generated between two CNT electrodes (upper curve in Fig. 2c). When the nanogenerator was turned over, the reversed current signal could reach the same amplitude (lower curve in Fig. 2c). The values of V_{oc} and I_{sc} fit well

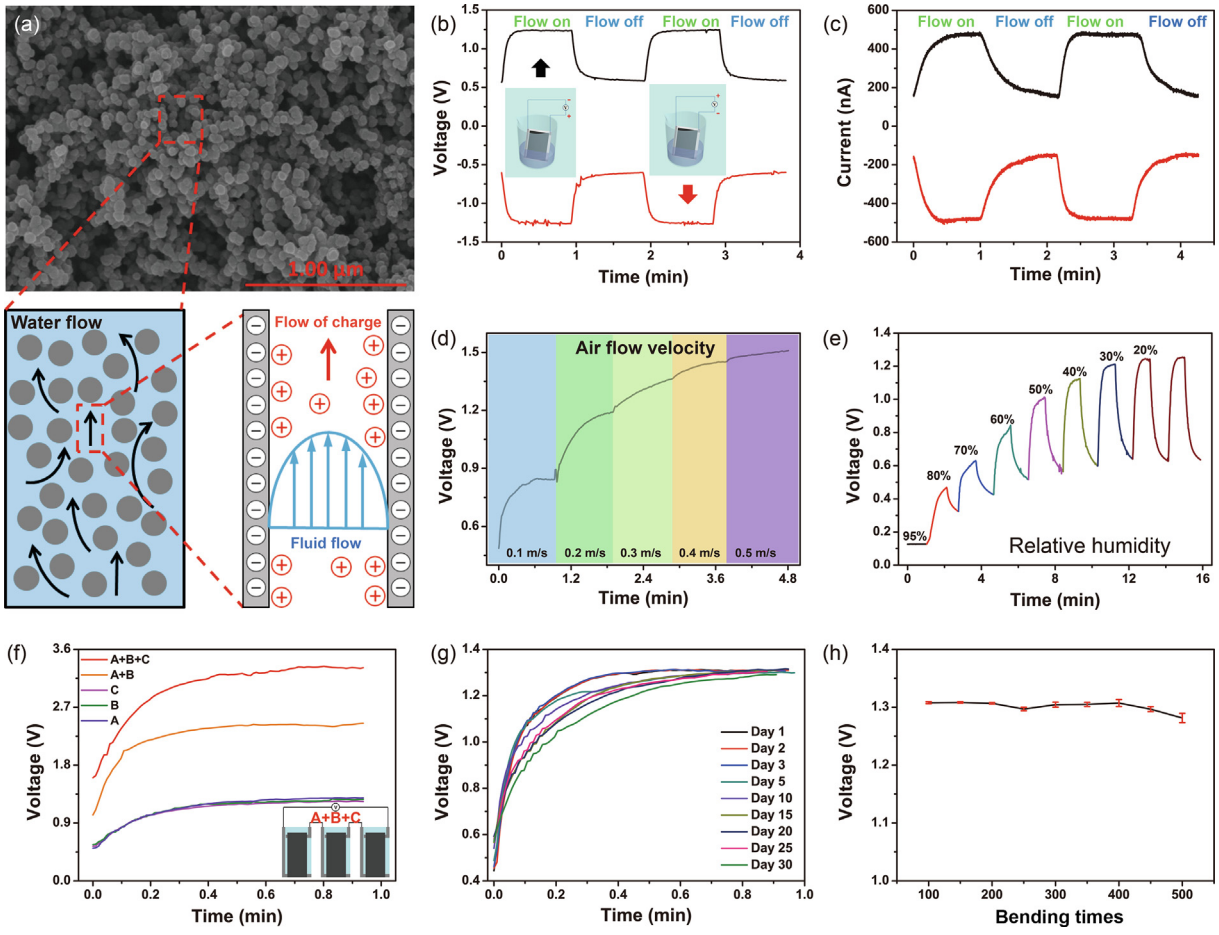

Fig. 2. (Color online) Electricity-generating behavior of water-evaporation-induced nanogenerator. (a) Working principle of water-evaporation-induced nanogenerator. V_{oc} (b) and I_{sc} (c) of the nanogenerator before (upper curve) and after (lower curve) turning upside down. (d) V_{oc} values at different airflow rates. (e) V_{oc} values under different RH. (f) V_{oc} values of three individual nanogenerators and them connected in series. (g) Stability of the nanogenerator. (h) V_{oc} value after repeated bending.

with the theoretical prediction based on the measured zeta potential.

When the nanogenerator was sealed within the beaker, the voltage (~1.2 V) dropped accordingly and finally approached zero. Upon unsealing the system again, the voltage rapidly returned to the original value (~1.2 V). This behavior was highly reproducible, as shown in Fig. S11 (online). Fluctuations in the output voltage and current could be attributed to changes in the environmental RH, air flow velocity, or water temperature during the tests. The voltage increased with increasing velocity of air flow, as shown in Fig. 2d. The relationship between the air flow velocity and voltage is shown in Fig. S12 (online). For air flow velocities of 0.1, 0.2, 0.3, 0.4, and 0.5 m/s, the voltage was 0.771, 1.190, 1.376, 1.463, and 1.486 V, respectively. Fig. 2e shows the output voltage of the nanogenerator at room temperature for different RH. The output voltage increased with decreasing RH. For a RH of 80%, 70%, 60%, 50%, 40%, 30%, and 20%, the voltage value was about 0.468, 0.629, 0.841, 1.013, 1.126, 1.211, and 1.243 V, respectively. As shown in Fig. S13 (online), the water temperature can slightly influence the output current. The output voltage was 1.192, 1.222, 1.254, 1.277, and 1.303 V for water temperatures of 18, 21, 25, 28, and 32 °C, respectively. These results indicate that water evaporation is the driving force for the electricity generation. Enhancing water evaporation leads to a high output voltage. In order to avoid any issues owing to the influence of the water temperature, all measurements were conducted at 25 °C. To further confirm the environmental influence on the output voltage, the nanogenerator was tested at different water depths. The bottom electrode of the nanogenerator was kept under the water level, and the top electrode was kept above the water level. Fig. S14 (online) shows the measures voltages for different water levels. For water depths of 1.5, 2.0, 2.5, 3.0, 3.5, and 4.0 cm, the voltage of the device was 1.233, 1.191, 1.108, 0.909, 0.594, and 0.436 V, respectively. With increase in the water level, the evaporation region became shorter and the voltage of the device decreased.

When two or three nanogenerators were connected in series, the voltage could reach up to 2.44 and 3.32 V, respectively (Fig. 2f). Figs. 2g, S15, and S16 (online) demonstrate the continuity and stability of the nanogenerator. These properties of the nanogenerator are essential for future applications. The output voltage could be sustained for 2 h and was constant during a thirty-day test, confirming the high stability of the nanogenerator. In the context of practical application, flexibility of the nanogenerator is a crucial parameter. Fig. 2h exhibits the voltage achieved after bending the device several times. The output voltage was stable during the test, confirming the high flexibility of the nanogenerator.

The electrochemical performance of the flexible nano-patterned supercapacitor was studied by employing a PVA/H_3PO_4 gel electrolyte in a two-electrode configuration. The CV curves obtained at a potential of 0–0.6 V and different scan rates are shown in Fig. 3a. Symmetrical and rectangular shapes were observed, and no appreciable redox peak was observed at the different scan rates.

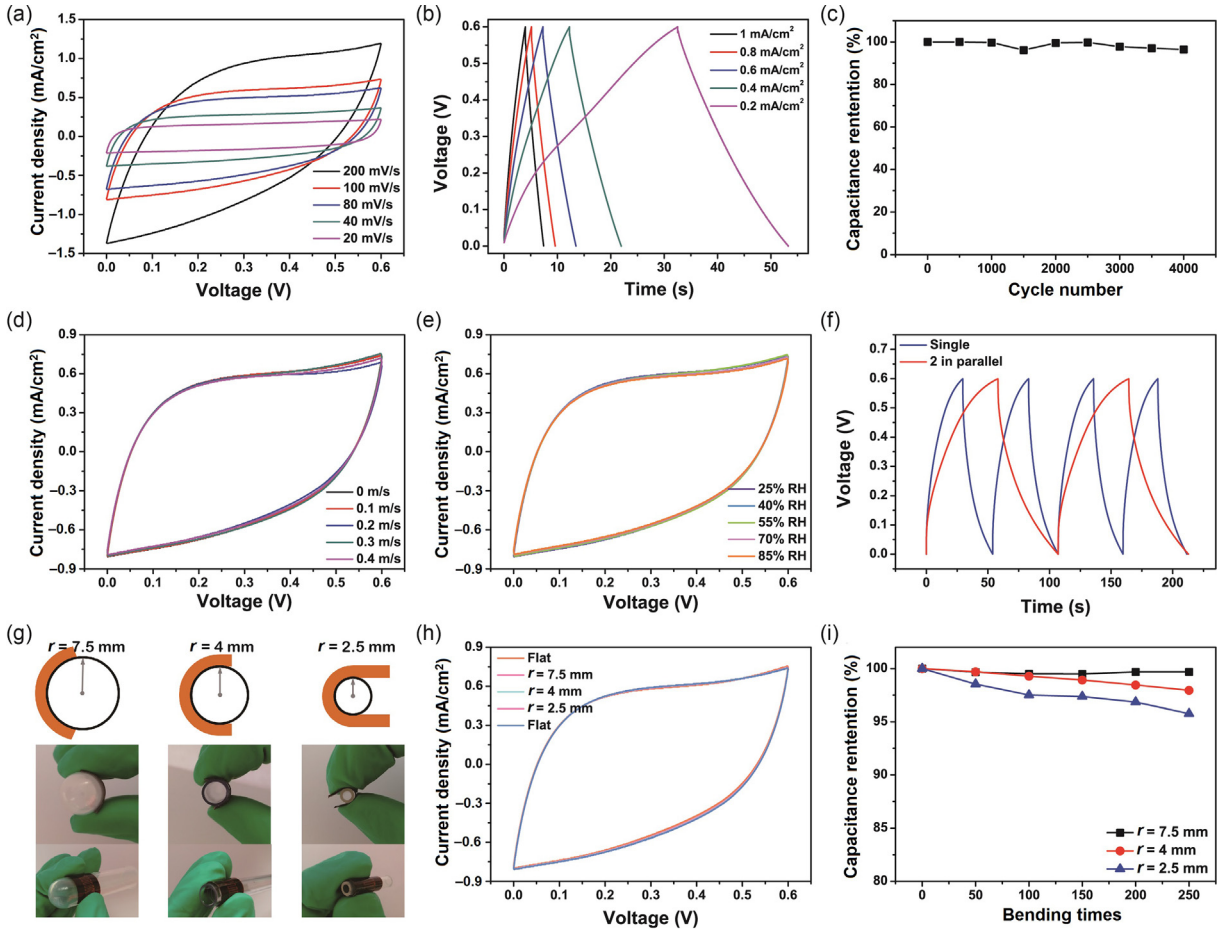

Fig. 3. (Color online) Electrochemical performance of Ppy-based nano-patterned supercapacitor. (a) CV curves of supercapacitor at different scan rates. (b) Galvanostatic charge/discharge curves at different current densities. (c) Cycling stability at scan rate of 100 mV/s. (d) CV curves under different airflow velocities. (e) CV curves under different RH. (f) Galvanostatic charge/discharge curves of the combined and individual supercapacitors. (g) The supercapacitor tested at different bending radii. (h) CV curves for the supercapacitor when flat state and after being bent. (i) Capacitance retention of the supercapacitor after 250 cycles at different bending radii.

This indicates good capacitive behavior. As seen in Fig. 3a, the areal capacitance reached a value of 14.871 mF/cm^2 at the scan rate of 20 mV/s. The areal capacitance was 12.497, 10.185, 9.377, and 6.622 mF/cm^2 at the scan rates of 40, 80, 100, and 200 mV/s, respectively. The galvanostatic charging/discharging (GCD) curves of the supercapacitor are presented in Fig. 3b. The curves are linear and show good symmetry in the potential window of 0–0.6 V, indicating excellent charge/discharge performance. Moreover, the internal resistance (IR) drop of the supercapacitor was merely 0.02 V at the current density of 0.2 mA/cm^2. Fig. 3c illustrates the cycling performance of the supercapacitor during 4,000 cycles at the scan rate of 100 mV/s. After 4,000 cycles, the capacity retention was 96.42%. Fig. 3d and e shows the CV curves of the supercapacitor under different air flow rates and different RH. The CV curves are almost the same at different states, demonstrating excellent cycling performance.

Fig. 3f shows that the capacitance of two supercapacitors (in parallel) was (almost twice) higher than that of a single

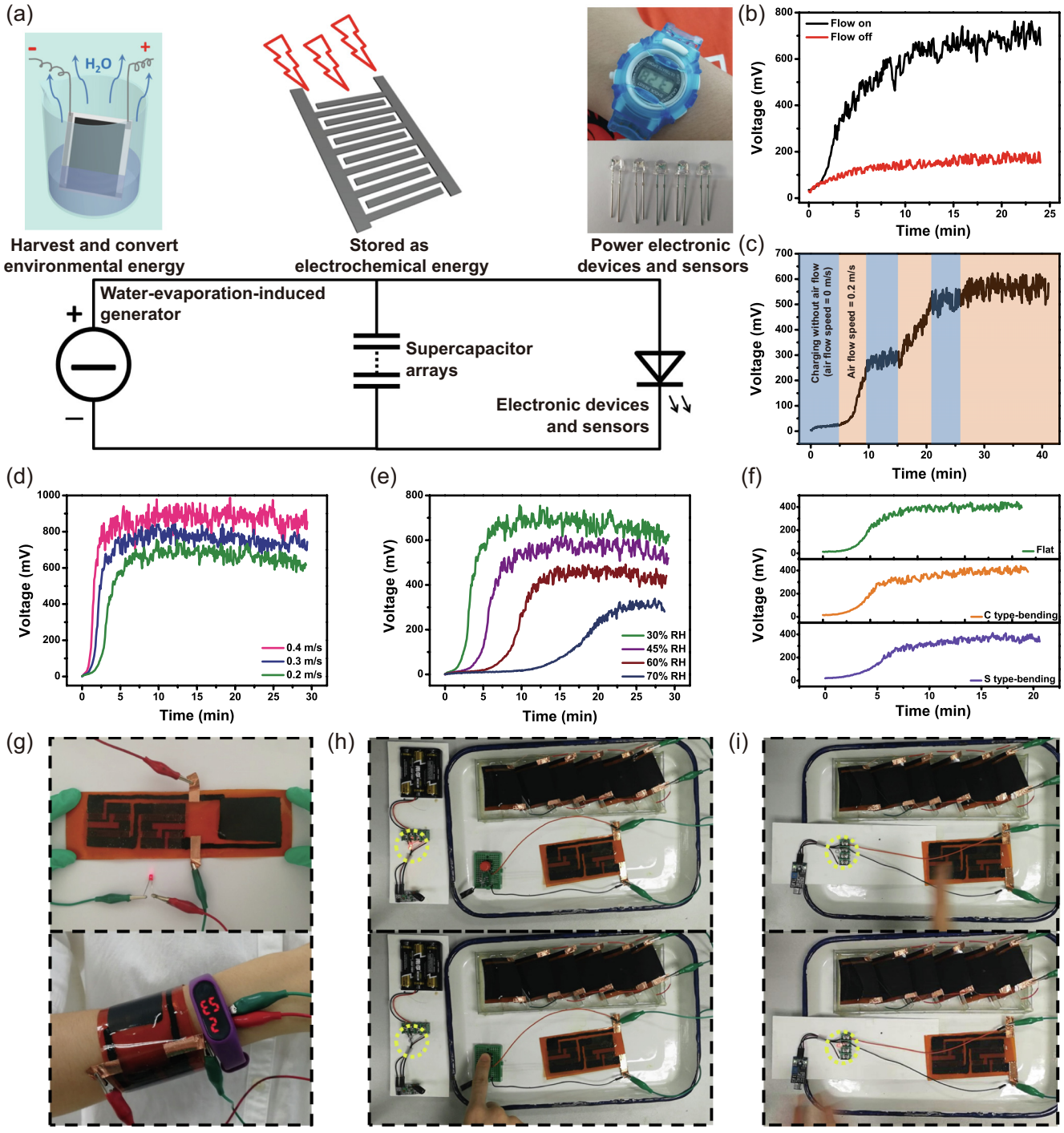

Fig. 4. (Color online) Self-charging behavior of self-powered hybrid power unit. (a) Equivalent electric circuit of the self-charging hybrid power unit. (b) Charging curve of the hybrid power unit at different airflow rates. (c) Charging curves in the presence and absence of airflow. (d–f) Charging curves under different conditions (airflow rate, RH, and bending type). (g) The hybrid power unit driving a common smart band. (h) The hybrid power unit powering a wireless transmission device to transmit a wireless signal. (i) The hybrid power unit driving a sound sensor for detecting clapping sound.

supercapacitor. In practical application, the flexibility and stability of the supercapacitor are crucial parameters. Fig. 3g presents the results acquired in the bending tests conducted on the flexible supercapacitor with the PDMS protective layer. The supercapacitor could be bent with bending radii of 7.5, 4, and 2.5 mm. In Fig. 3h, it can be seen that the CV curves show almost no change with variation in the bending radius of the supercapacitor, demonstrating high flexibility. As shown in Fig. 3i, 99.68%, 97.95%, and 95.76% of the specific capacitance were retained for the radii of 7.5, 4, and 2.5 mm after bending for 250 times, respectively.

The self-charging hybrid power unit can be integrated with sensor nodes and other electronic devices in the IoT, forming a self-sustainable battery-free data collection/submission system, as shown in Fig. 4a. The water-evaporation-induced nanogenerator can output electricity (DC) and the energy can be directly stored in the flexible supercapacitors. Furthermore, the supercapacitors can be connected together to fulfil the energy requirements of different electronic devices. Fig. 4b–f shows the self-charging behavior of the self-charging hybrid power unit under different environmental conditions. Fig. 4b shows that, at the airflow velocity of 0.3 m/s, the voltage of the hybrid power unit increased from 35 to 660 mV within 24 min. This self-charging process is very distinct. Here, the water could be treated as the fuel of the unit, which is charged by the environmental thermal and mechanical energy without the need for any external electricity power. In the absence of airflow, the voltage changed slightly from 30 to 150 mV. The self-charging and discharging processes of the hybrid power unit are shown in Fig. S17a (online). When the hybrid power unit was placed under an air speed of 0.3 m/s at 30% RH and 25 °C, the charge current was 0.48 μA (Fig. S17b online), the voltage of the unit increased from 97 to 513 mV within 10 min, and the charge noted was ~288 μC. After this self-charging process, the self-charging hybrid power unit was discharged back to its original voltage in 155 s under a constant discharge current of 1.8 μA. The actual amount (discharge capacity) of charge stored in the supercapacitor was 279 μC. As shown in Fig. 4c, the self-charging process of the hybrid power unit is directly related to the airflow. The charged voltage of the unit is dependent on both the airflow velocity and RH. The charged voltage was higher under a higher airflow velocity, as shown in Fig. 4d, and smaller under a higher RH, as shown in Fig. 4e. These factors can influence the output of the water-evaporation-induced nanogenerator. The hybrid power unit can function under different applied deformations, as shown in Fig. 4f. As the hybrid power unit was bent in a C-shape and an S-shape, the charged voltage and charging rate observed were similar to those for a flat shape.

The hybrid power unit can easily light a LED and drive a commercial smart band, as shown in Fig. 4g. The hybrid power unit can also power a wireless transmission device, as shown in Fig. 4h. Several water-evaporation-induced nanogenerators were connected in series to provide sufficient energy and linked to the supercapacitor to form a self-charging hybrid power unit. The hybrid power unit was directly linked to the wireless transmission device. The wireless receiver module consisted of LEDs, a diode, a receiving module, and power supply. The wireless transmission device could be powered by the hybrid power unit, and it could transmit a wireless signal when the button was pressed. The receiver module received the signal and turned off the LED for a while, and then the lights turned on again. The entire process is shown in Movie S1 (online). The hybrid power unit could also drive a sound node (3 V) for detecting sound waves, as shown in Fig. 4i. The hybrid power unit, which consisted of several nanogenerators connected in series and a supercapacitor, was linked to the sound sensor, and the sensor began to operate. When the tester clapped their hands near the sensor, the sensor could detect the sound and the LED could be turned on. When the sound faded, the LED turned off. This process is demonstrated in detail in Movie S2 (online). It should be noted that the capacitance of the hybrid power unit needs to be enhanced, the voltage of the nanogenerator needs to be increased, and the stability of the output voltage needs to be improved so that a wider variety of materials (polythiophene and carbon composite structures) can be applied in this hybrid power unit to achieve excellent performance in future [58–61].

4. Conclusion

In summary, a water-evaporation-induced self-charging hybrid power unit has been developed by integrating a water-evaporation-induced nanogenerator with a flexible nano-patterned supercapacitor. The self-charging hybrid power unit can directly harvest environmental thermal and mechanical energy through water evaporation, and the energy can be spontaneously stored as electrochemical energy without significant energy waste. The output performance of the nanogenerator was stable and efficient, and the capacitance of the supercapacitor was 12.497 mF/cm^2 with 96.42% retention after 4,000 cycles. The hybrid power unit is very environmentally friendly, and the water can be directly used as fuel. The hybrid power unit as the power supply can be easily integrated with various electronic devices in the IoT. This new approach offers great potential for solving issues pertaining to energy supply in randomly distributed electronic devices in the IoT and could therefore contribute to further development of the IoT. In future work, the capacitance of the hybrid power unit needs to be enhanced, the voltage of the nanogenerator needs to be increased, and the stability of the output voltage needs to be improved so that different materials (polythiophene and carbon composite structures) can be employed in such power units toward excellent performance.

Conflict of interest

The authors declare that they have no conflict of interest.

Acknowledgments

This work was supported by the National Natural Science Foundation of China (11674048), the Fundamental Research Funds for the Central Universities (N170505001, and N160502002), and Program for Shenyang Youth Science and Technology Innovation Talents (RC170269).

Author contributions

X. Xue, Y. Zhang, and L. Xing devised the concept. X. Xue and H. He designed the experiments. H. He, H. Zeng, and T. Zhao performed the experiments. X. Xue, H. He, and Y. Zhang analyzed the data. H. Guan, T. Zhong, and H. He characterized the materials. X. Xue, H. He, and L. Xing wrote the manuscript. All the authors contributed to the general discussion.

Appendix A. Supplementary data

Supplementary data to this article can be found online at https://doi.org/10.1016/j.scib.2019.06.020.

References

[1] Chen YL, Wang YC, Zhang Y, et al. Elastic-beam triboelectric nanogenerator for high-performance multifunctional applications: sensitive scale, acceleration/force/vibration sensor, and intelligent keyboard. Adv Energy Mater 2018;8:1802159.

[2] Wang ZL. On maxwell's displacement current for energy and sensors: the origin of nanogenerators. Mater Today 2017;20:74–82.
[3] Wang ZL, Chen J, Lin L. Progress in triboelectric nanogenerators as a new energy technology and self-powered sensors. Energy Environ Sci 2015;8:2250–82.
[4] Wang SH, Lin L, Wang ZL. Triboelectric nanogenerators as self-powered active sensors. Nano Energy 2015;11:436–62.
[5] Wang ZL, Song JH. Piezoelectric nanogenerators based on zinc oxide nanowire arrays. Science 2006;312:242–6.
[6] Xu S, Qin Y, Xu C, et al. Self-powered nanowire devices. Nat Nanotechnol 2010;5:366–73.
[7] Li SS, Cheng PP, Luo JX, et al. High-performance flexible asymmetric supercapacitor based on CoAl-LDH and rGO electrodes. Nano Micro Lett 2017;9:31.
[8] Fu YM, He HX, Zhao TM, et al. A self-powered breath analyzer based on PANI/PVDF piezo-gas-sensing arrays for potential diagnostics application. Nano Micro Lett 2018;10:76.
[9] Dong YF, Wu ZS, Ren WC, et al. Graphene: a promising 2D material for electrochemical energy storage. Sci Bull 2017;62:724–40.
[10] Zhao C, Zhang Q, Zhang W, et al. Hybrid piezo/triboelectric nanogenerator for highly efficient and stable rotation energy harvesting. Nano Energy 2019;57:440–9.
[11] Shao HY, Cheng P, Chen RX, et al. Triboelectric-electromagnetic hybrid generator for harvesting blue energy. Nano Micro Lett 2018;10:54.
[12] Lai YC, Hsiao YC, Wu HM, et al. Waterproof-fabric-based multifunctional triboelectric nanogenerator for universally harvesting energy from raindrops, wind, and human motions and as self-powered sensors. Adv Sci 2019;6:1801883.
[13] Zhang WLH, Zhang LL, Gao HL, et al. Self-powered implantable skin-like glucometer for real-time detection of blood glucose level in vivo. Nano Micro Lett 2018;10:32.
[14] Zhang JJ, Yu AS. Nanostructured transition metal oxides as advanced anodes for lithium-ion batteries. Sci Bull 2015;60:823–38.
[15] Wang ZL. Toward self-powered sensor networks. Nano Today 2010;5:512–4.
[16] Niu SM, Wang XF, Yi F, et al. A universal self-charging system driven by random biomechanical energy for sustainable operation of mobile electronics. Nat Commun 2015;6:8975.
[17] Liang JJ, Yuan CC, Li HH, et al. Growth of SnO_2 nanoflowers on N-doped carbon nanofibers as anode for Li- and Na-ion batteries. Nano Micro Lett 2018;10:21.
[18] Candelaria SL, Cao GZ. Increased working voltage of hexamine-coated porous carbon for supercapacitors. Sci Bull 2015;60:1587–97.
[19] Mo FN, Li HF, Pei ZX. A smart safe rechargeable zinc ion battery based on sol-gel transition electrolytes. Sci Bull 2018;63:1077–86.
[20] Guo HY, Yeh MH, Lai YC, et al. All-in-one shape-adaptive self-charging power package for wearable electronics. ACS Nano 2016;10:10580–8.
[21] Wang XF, Liu B, Liu R, et al. Fiber-based flexible all-solid-state asymmetric supercapacitors for integrated photodetecting system. Angew Chem Int Ed 2014;53:1849–53.
[22] Yue Y, Yang ZC, Liu NS, et al. A flexible integrated system containing a microsupercapacitor, a photodetector, and a wireless charging coil. ACS Nano 2016;10:11249–57.
[23] He HX, Zeng H, Fu YM, et al. A self-powered electronic-skin for real-time perspiration analysis and application in motion state monitoring. J Mater Chem C 2018;6:9624–30.
[24] Zeng H, He HX, Fu YM, et al. A self-powered brain-linked biosensing electronicskin for actively tasting beverage and its potential application in artificial gustation. Nanoscale 2018;10:19987–94.
[25] Zhu G, Chen J, Liu Y, et al. Linear-grating triboelectric generator based on sliding electrification. Nano Lett 2013;13:2282–9.
[26] Dai YT, Fu YM, Zeng H, et al. A self-powered brain-linked vision electronic-skin based on triboelectric-photodetecing pixel-addressable matrix for visual-image recognition and behavior intervention. Adv Funct Mater 2018;28:1800275.
[27] Fu YM, Zhang MY, Dai YT, et al. A self-powered brain multi-perception receptor for sensory-substitution application. Nano Energy 2018;44:43–52.
[28] He HX, Fu YM, Zang WL, et al. A flexible self-powered T-ZnO/PVDF/fabric electronic-skin with multi functions of tactile-perception, atmosphere-detection and self-clean. Nano Energy 2017;31:37–48.
[29] Xue XY, Qu Z, Fu YM, et al. Self-powered electronic-skin for detecting glucose level in body fluid basing on piezo-enzymatic-reaction coupling process. Nano Energy 2016;26:148–56.
[30] Xue XY, Fu YM, Wang Q, et al. Outputting olfactory bionic electric impulse by PANI/PTFE/PANI sandwich nanostructures and their application as flexible, smelling electronic skin. Adv Funct Mater 2016;26:3128–38.
[31] Wen Z, Shen QQ, Sun XH. Nanogenerators for self-powered gas sensing. Nano Micro Lett 2017;9:45.
[32] Xue GB, Xu Y, Ding TP, et al. Water-evaporation-induced electricity with nanostructured carbon materials. Nat Nanotechnol 2017;12:317–21.
[33] Ding TP, Liu K, Li J, et al. All-printed porous carbon film for electricity generation from evaporation-driven water flow. Adv Funct Mater 2017;27:1700551.
[34] Zhong TY, Guan HY, Dai YT, et al. A self-powered flexibly-arranged gas monitoring system with evaporating rainwater as fuel for building atmosphere big data. Nano Energy 2019;60:52–60.
[35] Guan HY, Zhong TY, He HX, et al. A self-powered wearable sweat-evaporation-biosensing analyzer for building sports big data. Nano Energy 2019;59:754–61.
[36] McCulloh KA, Sperry JS, Adler FR. Water transport in plants obeys murray's law. Nature 2003;421:939–42.
[37] Kurra N, Jiang Q, Alshareefn HN. A general strategy for the fabrication of high performance microsupercapacitors. Nano Energy 2015;16:1–9.
[38] Xia HC, Zhang JN, Yang Z. 2D MOF nanoflake-assembled spherical microstructures for enhanced supercapacitor and electrocatalysis performances. Nano Micro Lett 2017;9:43.
[39] Liu HB, Tian YH, Amal R, et al. An integrated nanocarbon-cellulose membrane for solid-state supercapacitors. Sci Bull 2016;61:368–77.
[40] Wang CG, Guo K, He WD, et al. Hierarchical $CuCo_2O_4$@nickel-cobalt hydroxides core/shell nanoarchitectures for high-performance hybrid supercapacitors. Sci Bull 2017;62:1122–31.
[41] Tao JY, Ma WZ, Liu NS, et al. High-performance solid-state supercapacitors fabricated by pencil drawing and polypyrrole depositing on paper substrate. Nano Micro Lett 2015;7:276–81.
[42] Huang Y, Huang Y, Zhu MS, et al. Magnetic-assisted, self-healable, yarn-based supercapacitor. ACS Nano 2015;9:6242–51.
[43] Zhao K, Wang YH, Han L, et al. Nanogenerator-based self-charging energy storage devices. Nano Micro Lett 2019;11:19.
[44] Wang SH, Lin ZH, Niu SM, et al. Motion charged battery as sustainable flexible-power-unit. ACS Nano 2013;7:11263–71.
[45] Guo WX, Xue XY, Wang SH, et al. An integrated power pack of dye-sensitized solar cell and li battery based on double-sided TiO_2 nanotube arrays. Nano Lett 2012;12:2520–3.
[46] Xue XY, Wang SH, Guo WX, et al. Hybridizing energy conversion and storage in a mechanical-to-electrochemical process for self-charging power cell. Nano Lett 2012;12:5048–54.
[47] Xue XY, Deng P, Yuan S, et al. CuO/PVDF nanocomposite anode for a piezo-driven self-charging lithium battery. Energy Environ Sci 2013;6:2615–20.
[48] Zhang Y, Zhang YJ, Xue XY, et al. PVDF-PZT nanocomposite film based self-charging power cell. Nanotechnology 2014;25:105401.
[49] Xue XY, Deng P, He B, et al. Flexible self-charging power cell for one-step energy conversion and storage. Adv Energy Mater 2014;4:1301329.
[50] Xing LL, Nie YX, Xue XY, et al. PVDF mesoporous nanostructures as the piezo-separator for a self-charging power cell. Nano Energy 2014;10:44–52.
[51] He HX, Fu YM, Zhao TM. All-solid-state flexible self-charging power cell basing on piezo-electrolyte for harvesting/storing body-motion energy and powering wearable electronics. Nano Energy 2017;39:590–600.
[52] He HX, Dong CY, Fu YM, et al. Self-powered smelling electronic-skin based on the piezo-gas-sensor matrix for real-time monitoring the mining environment. Sens Actuators B Chem 2018;267:392–402.
[53] Kim DH, Viventi J, Amsden JJ, et al. Dissolvable films of silk fibroin for ultrathin conformal bio-integrated electronics. Nat Mater 2010;9:511–7.
[54] Duffin AM, Saykally RJ. Electrokinetic hydrogen generation from liquid water microjets. J Phys Chem C 2007;111:12031–7.
[55] Zhang R, Wang SH, Yeh MH, et al. A streaming potential/current-based microfluidic direct current generator for self-powered nanosystems. Adv Mater 2015;27:6482–7.
[56] Zhang L, Chen XD. Nanofluidics for giant power harvesting. Angew Chem Int Ed 2013;52:7640–1.
[57] Liu K, Ding TP, Li J, et al. Thermal-electric nanogenerator based on the electrokinetic effect in porous carbon film. Adv Energy Mater 2018;8:1702481.
[58] Snook GA, Kao P, Best AS. Conducting-polymer-based supercapacitor devices and electrodes. J Power Source 2011;196:1–12.
[59] Meng QF, Cai KF, Chen YX, et al. Research progress on conducting polymer based supercapacitor electrode materials. Nano Energy 2017;36:268–85.
[60] Ji BX, Chen N, Shao CX, et al. Intelligent multiple-liquid evaporation power generation platform using distinctive Jaboticabalike carbon nanosphere@TiO_2 nanowires. J Mater Chem A 2019;7:6766–72.
[61] Li J, Liu K, Ding TP, et al. Surface functional modification boosts the output of an evaporation-driven water flow nanogenerator. Nano Energy 2019;58:797–802.

Haoxuan He is currently studying for the doctor degree in the College of Sciences, Northeastern University, China. His research interests focus on the self-powered sensor, self-powered electronic skin and self-charging power unit system.

Lili Xing is a Professor at the University of Electronic Science and Technology of China. She mainly focuses on the synthesis of metal oxide nanostructures.

Xinyu Xue is a Professor at University of Electronic Science and Technology of China and College of Sciences, Northeastern University, China. Currently he is working on the next generation of sensors and batteries, such as self-powered active sensors and self-charging lithium battery.